

# The image separation distribution of strong lenses: Halo versus subhalo populations

Masamune Oguri<sup>1,2\*</sup>

<sup>1</sup>*Princeton University Observatory, Peyton Hall, Princeton, NJ 08544, USA.*

<sup>2</sup>*Department of Physics, University of Tokyo, Hongo 7-3-1, Bunkyo-ku, Tokyo 113-0033, Japan.*

7 February 2020

## ABSTRACT

We present a halo model prediction of the image separation distribution of strong lenses. Our model takes account of the subhalo population, which has been ignored in previous studies, as well as the conventional halo population. Halos and subhalos are linked to central and satellite galaxies by adopting an universal scaling relation between masses of (sub-)halos and luminosities of galaxies. Our model predicts that 10%–20% of lenses should be caused by the subhalo population. The fraction of lensing by satellite galaxies (subhalos) peaks at  $\sim 1''$  and decreases rapidly with increasing image separations. We compute fractions of lenses which lie in groups and clusters, and find them to be  $\sim 14\%$  and  $\sim 4\%$ , respectively: Nearly half of such lenses are expected to be produced by satellite galaxies, rather than central parts of halos. We also study mass distributions of lensing halos and find that even at image separations of  $\sim 3''$  the deviation of lens mass distributions from isothermal profiles is large: At or beyond  $\sim 3''$  image separations are enhanced significantly by surrounding halos. Our model prediction agrees reasonably well with observed image separation distributions from galaxy to cluster scales.

**Key words:** cosmology: theory — dark matter — galaxies: elliptical and lenticular, cD — galaxies: formation — galaxies: halos — galaxies: clusters: general — gravitational lensing

## 1 INTRODUCTION

Image separations between multiple images play an important role in the statistics of lensed quasars: The image separation is mainly determined by the potential well depth of the lens object, thus the image separation distribution reflects hierarchical structure in the universe. This fact suggests that lensed quasars may be categorized roughly into two populations; small-separation lens ( $\theta \sim 1''$ ) that are produced by a single galaxy, and a large-separation lens ( $\theta \gtrsim 10''$ ) that are caused by clusters of galaxies. Thus far about 80 lensed quasars are known: Most are small-separation lenses and only one lens, SDSS J1004+4112 (Inada et al. 2003; Oguri et al. 2004), has the image separation larger than  $10''$ . The current largest homogeneous lens survey, the Cosmic Lens All Sky Survey (CLASS; Myers et al. 2003; Browne et al. 2003), contains small separation only, thus it may not be suitable for studying the image separation distribution from galaxy to cluster scales. However, ongoing lens surveys such as that in the Sloan Digital Sky Survey (SDSS) are expected to unveil the full distribution, which

will be extremely useful for understanding the assembly of structures.

In theoretical sides, there have been many attempts to calculate the full image separation distribution. Historically, the image separation distribution is computed from either the galaxy luminosity function (Turner et al. 1984) or the mass function of dark halos (Narayan & White 1988). While the former approach accounts for the observed lensing probability and its distribution at  $\theta < 3''$  fairly well, it has difficulty in explaining the existence of the large-separation lens for which dark matter dominates the lens potential. Therefore in this paper we take the latter approach.

However, modeling the image separation distribution on the basis of dark halos is not simple. It has been found that none of models that consider only one population for lensing halos are consistent with current observations. Correct models need to include a characteristic mass around  $M_{\text{cool}} \sim 10^{13} M_{\odot}$ , where the density distribution inside dark halos changes (Porciani & Madau 2000; Kochanek & White 2001; Keeton 2001; Sarbu et al. 2001; Li & Ostriker 2002, 2003; Oguri 2002; Ma 2003; Huterer & Ma 2004; Kuhlen et al. 2004; Chen 2004; Zhang 2004; Chen 2005; Zhang et al. 2005): Large mass halos  $M > M_{\text{cool}}$  (correspond to groups

\* E-mail:oguri@astro.princeton.edu

or clusters) have cooling time longer than the Hubble time, thus the internal structure of dark halos is not strongly affected by baryon cooling and is well described by that of dark matter (Navarro et al. 1997). On the other hand, in small mass halos  $M < M_{\text{cool}}$  (correspond to galaxies) the baryon cooling is very efficient and the mass distribution becomes strongly centrally concentrated, which is well approximated by the Singular Isothermal Sphere (SIS). Although this two-component model is successful in explaining the image separation distribution to some extent, clearly it is not sufficient. First of all, this model considers only galaxies that lie at the center of isolated dark halos, and thus does not take galaxies in groups and clusters into account. Put another way, this model neglects substructures (subhalos) which should correspond to satellite galaxies. Actually, it has been speculated that lens systems in such dense environments is quite common (Keeton et al. 2000). In addition, sometimes lens systems are significantly affected by the mass distribution outside the lens object. A good example is Q0957+561 (Walsh et al. 1979); its lens object is a galaxy in a cluster, and the image separation is much larger than expected from the luminosity of the lens galaxy because the image separation is boosted by the cluster potential. Indeed, it has been shown theoretically that at intermediate-separation regime ( $\theta = 3'' - 7''$ ) lens galaxies in dense environments are quite common (Oguri et al. 2005). Therefore the correct model needs to account for such external mass.

To construct a model that is based on dark halos and subhalos, we have to model the relation between mass of dark halos (subhalos) and luminosities of galaxies inside them. There are several models to link them: Conditional luminosity function (CLF) which is defined by the luminosity function in a halo of given mass (Yang et al. 2003; van den Bosch et al. 2005), universal mass-luminosity relation between halo/subhalo mass and hosted galaxy luminosity (Vale & Ostriker 2004), and the mixture of these two models (Cooray & Milosavljević 2005; Cooray & Cen 2005). There models are calibrated to match observed galaxy luminosity functions, clustering of galaxies as a function of galaxy luminosities, and the luminosity function of galaxies in groups or clusters.

In this paper, we study the image separation distribution with a particular emphasis on the different contributions from central and satellite galaxies. For central galaxies, we consider baryon cooling in a dark matter halo as done by Kochanek & White (2001) and Keeton (2001). Satellite galaxies, which have been neglected in previous studies, are linked to dark halo substructures. We basically take the approach proposed by Vale & Ostriker (2004) to relate mass of dark halos and subhalos with luminosities of galaxies, but we modify it to account for the relatively small abundance of satellite galaxies in galactic halos (see Cooray & Cen 2005). For satellite galaxies, the external mass from the host halo, which is shown to be important at large-image separations, is taken into account. In addition to the difference between central and satellite galaxies, we also pay particular attention to how lens objects make the transition from SIS to NFW as halo masses increase.

This paper is organized as follows. In §2, we introduce models of dark halos and subhalos that are used to compute lensing probabilities. Section 3 are devoted to model the relation between (sub-)halo masses and galaxy luminosities.

We compute the image separation distributions in §4, and show the results in §5. Finally, we summarize and discuss our results in §6. Throughout the paper we assume a concordance cosmology with the mass density  $\Omega_M = 0.3$ , the cosmological constant  $\Omega_\Lambda = 0.7$ , the dimensionless Hubble parameter  $h = 0.7$ , and the normalization of the mass fluctuation  $\sigma_8 = 0.9$ .

## 2 MODELING DARK HALOS AND SUBHALOS

### 2.1 Dark Halos

For the density profile of original dark halos, we adopt the spherical NFW profile (Navarro et al. 1997):

$$\rho(r) = \frac{\rho_s}{(r/r_s)(1+r/r_s)^2}. \quad (1)$$

The characteristic density  $\rho_s$  is computed from the nonlinear overdensity  $\Delta_{\text{vir}}$ . The scale radius  $r_s$  is related to the concentration parameter  $c = r_{\text{vir}}/r_s$ , where  $r_{\text{vir}}$  is the virial radius. The median concentration parameter depends on the mass  $M$  and redshift  $z$  of the dark halo: We adopt the fitting form derived by Bullock et al. (2001):

$$\bar{c} = \frac{10}{1+z} \left( \frac{M}{M_*} \right)^{-0.13}, \quad (2)$$

where  $M_*$  is determined by solving  $\sigma_M = \delta_c$  at  $z = 0$  ( $\sigma_M$  is the standard deviation of linear density field smoothed with a top-hat filter enclosing mass  $M$ , and  $\delta_c \approx 1.68$  is the threshold linear overdensity above which the region collapses). We also include the scatter in the concentration parameter, which is well described by a log-normal distribution:

$$p(c) = \frac{1}{\sqrt{2\pi}\sigma_{\ln c}c} \exp \left[ -\frac{(\ln c - \ln \bar{c})^2}{2\sigma_{\ln c}^2} \right], \quad (3)$$

where the standard deviation is  $\sigma_{\ln c} = 0.3$ .

In this paper, we consider the modification of mass distribution in dark halos due to baryon cooling. Traditionally, the response of dark matter to baryon infall has been calculated by the model of adiabatic contraction (Blumenthal et al. 1986). The model assumes the spherical symmetry and computes the response by imposing the conservation of angular momentum between before and after baryon infall. Recently, Gnedin et al. (2004) studies the validity of the model using high-resolution numerical simulations, and found that the model can be improved by taking the eccentric orbits of particles into account. They also presented a series of analytic fitting functions which make it much easier to implement the modification. We adopt this modified adiabatic compression model to derive the total mass distribution. For the final mass distribution of the cooled baryonic component, we assume Hernquist (1990) profile:

$$\rho_b(r) = \frac{M_b}{2\pi} \frac{1}{(r/r_b)(r_b+r)^3}, \quad (4)$$

which is known to describe the stellar density profile of elliptical galaxies well. Note that to compute the final mass distribution we need to specify the cooled mass  $M_b$  (or equivalently mass fraction  $f_b \equiv M_b/M$ ) and the core radius  $r_b$  (or

equivalently the ratio of the core radius to the scale radius  $x_b \equiv r_b/r_s$ ), in addition to halo parameters such as  $c$  and  $M$ .

For the mass function of dark halos, we use the form proposed by Sheth & Tormen (1999):

$$\frac{dn}{dM} = \frac{\rho(z) d \ln \sigma_M^{-1}}{M^2 d \ln M} \quad (5)$$

$$\times A \sqrt{\frac{2a}{\pi}} \left[ 1 + \left( \frac{\sigma_M^2}{a \delta_c^2} \right)^p \right] \frac{\delta_c}{\sigma_M} \exp \left[ -\frac{a \delta_c^2}{2 \sigma_M^2} \right], \quad (6)$$

where  $\rho(z)$  is the mean matter density at redshift  $z$ ,  $A = 0.322$ ,  $a = 0.707$ , and  $p = 0.3$ . The mass function is the modification of Press & Schechter (1974) to account for ellipsoidal nature of gravitational collapse in cosmological situations, and is known to reproduce the mass distribution and its redshift evolution in numerical simulations (e.g., Reed et al. 2003).

## 2.2 Subhalos

We consider subhalos which lie in a dark halo with mass  $M$ . The mass of the subhalo is denoted by  $m_s$  and the distance from the halo center by  $r$ . We always adopt an SIS for the density distribution of galaxies associated with subhalos for simplicity. Indeed it has been known that the central part of the density profile of total (dark matter plus cooled baryon) matter in a dark halo after baryon infall is quite close to an SIS. For the mass and spatial distributions of subhalos, we use a model constructed by Oguri & Lee (2004). In the paper, they showed that the analytic model reproduces well the results of high-resolution numerical simulations. In reality, we use the following fitting formulae of mass and spatial distributions to speed up the computation.

The fitting function of the number distribution of substructures was given by Vale & Ostriker (2004):

$$\frac{dN}{dm_s} = \frac{0.18}{\gamma \Gamma(2-\beta)} \left( \frac{m_s}{\gamma M} \right)^{-\beta} \exp \left( -\frac{m_s}{\gamma M} \right) \frac{1}{\gamma M}, \quad (7)$$

where  $\beta = 1.91$  and  $\gamma = 0.39$ . The mass function has a power-law form at  $m_s \ll M$ , and has a sharp cut-off at  $m_s \sim M$ . In addition, we assume that  $dN/dm_s = 0$  at  $m_s > M$ . We compare this fitting function with the result of Oguri & Lee (2004) in Figure 2, confirming the good accuracy of the fitting function.

It has been shown that the radial number density distributions of subhalos are less centrally concentrated relative to the dark matter particle components. Moreover, they depend on masses of subhalos: More massive subhalos are preferentially located in the external regions of their host halos (De Lucia et al. 2004; Oguri & Lee 2004; Gao et al. 2004). We find that the spatial distribution of subhalos is described by an NFW profile (eq. [1]) with different concentration parameter (which depend on  $m_s$ ) from that of the host halo. Specifically, the concentration parameter of the radial distribution of subhalos is fitted by

$$c^* = c \left[ 1 + \left( \frac{3m_s/M}{10^{-7}} \right)^{0.2} \right]^{-1}, \quad (8)$$

where  $c$  is the concentration parameter of the corresponding host halo. Figure 2 shows the comparison of this fitting

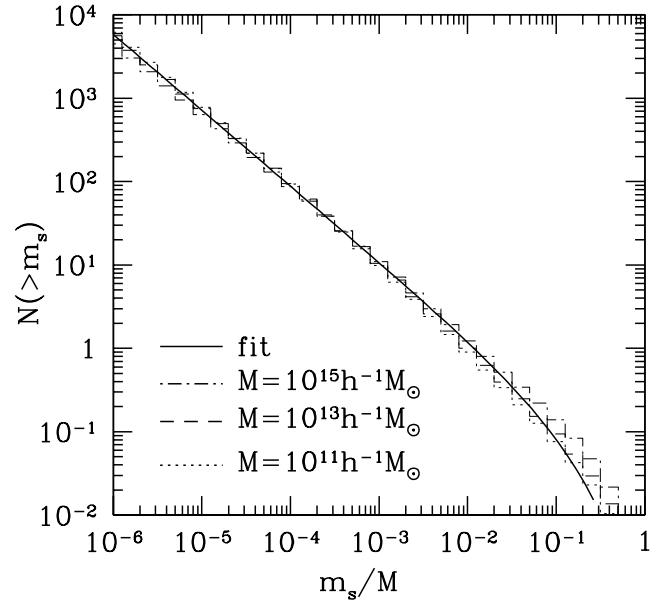


**Figure 1.** The comparison of the cumulative number distributions of subhalos derived from an analytic model of Oguri & Lee (2004) with the fitting function (obtained by integrating equation (7) over  $m_s$ ). The former is shown by histograms, and the latter is plotted by a solid line. We plot the distributions of the analytic model for three different masses of the host halos. Note that the cumulative mass distribution derived from the fitting function does not depend on the mass of the host halo when it is plotted as a function of  $m_s/M$ .

with the model of Oguri & Lee (2004). They agree reasonably well with each other for a range of parameters we are interested in.

## 3 LINKING DARK HALOS AND SUBHALOS TO GALAXIES

We consider a central galaxy with luminosity  $L$  which resides in a dark halo with mass  $M$ . We adopt the mass-luminosity ( $b_J$  band) relation proposed by Vale & Ostriker (2004):

$$L(M) = 5.7 \times 10^9 h^{-2} L_\odot \frac{M_{11}^p}{\left[ q + M_{11}^{(p-r)s} \right]^{1/s}}, \quad (9)$$

where  $p = 4$ ,  $q = 0.57$ ,  $r = 0.28$ ,  $s = 0.23$ , and  $M_{11} \equiv M/(10^{11} h^{-1} M_\odot)$ . Basically this relation asymptote to  $L \propto M^4$  at low mass end and  $L \propto M^{0.28}$  at high mass end. Vale & Ostriker (2004) claimed that the same relation can be applied to dark halo substructures (with mass  $m_s$ ) and satellite galaxies (with luminosity  $L_s$ ):

$$L_s(m_s) = 5.7 \times 10^9 h^{-2} L_\odot \frac{m_{11}^p}{\left[ q + m_{11}^{(p-r)s} \right]^{1/s}}, \quad (10)$$

where  $m_{11} \equiv m/(10^{11} h^{-1} M_\odot)$  and  $m$  is the mass of subhalos before the tidal stripping of the outer part of subhalos. We adopt the approximation relation  $m = 3m_s$ , which was also assumed in Vale & Ostriker (2004), throughout the paper for simplicity.

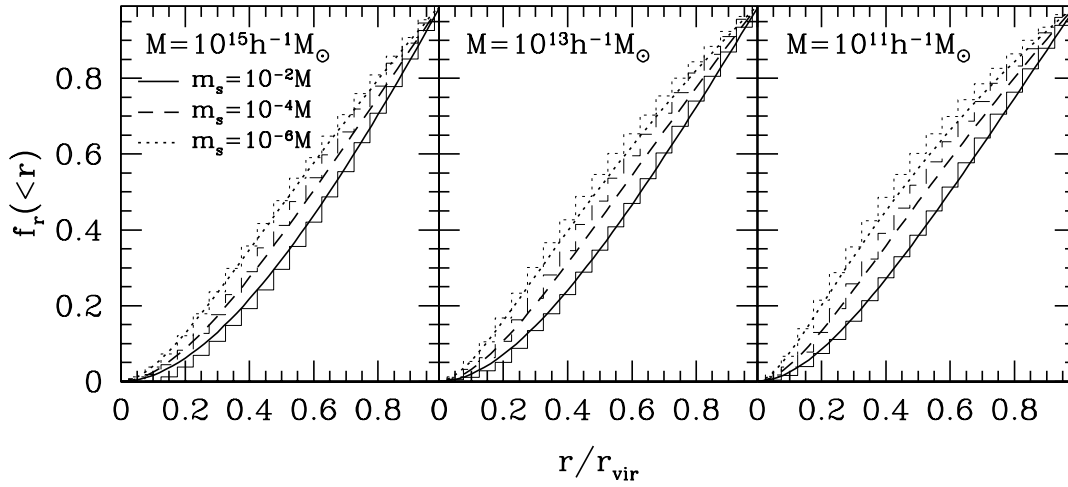


**Figure 2.** The cumulative radial distributions of subhalos in an analytic model (Oguri & Lee 2004) are compared with those of an NFW fit with concentration parameters given by equation (8). The former distributions are plotted with histograms, while the latter are shown by curves. From left to right panels, we change the mass of the host halo. Different lines indicate different masses of subhalos.

While Vale & Ostriker (2004) adopted monotonic one-to-one correspondence between halo/subhalo masses and resident galaxy luminosities, Cooray & Milosavljević (2005) showed that it is essential to assign log-normal scatter to the mass-luminosity relations to recover the tail of the observed luminosity function. Following them, we assume the log-normal luminosity distribution of

$$p(L|M) = \frac{1}{\sqrt{2\pi} \ln(10)\Sigma L} \exp\left\{-\frac{\log_{10}[L/L(M)]^2}{2\Sigma^2}\right\}, \quad (11)$$

with  $\Sigma = 0.25$ , and the same distribution with mean of  $L_s(m_s)$  for  $L_s$ .

Although this model is successful in explaining many observations such as the occupation number, the luminosity function of clusters and the group luminosity function, it cannot reproduce the strong dependence of the faint end slope of the CLF on the halo mass: Observationally, it changes from  $\sim -1.2$  at the cluster scale to  $\sim 0$  at galactic scales. Since the mass function of subhalos at low mass is  $dn/dm_s \propto m_s^{-\beta}$  where  $\beta \sim 1.9$  (see §2.2), the mass-luminosity relation  $L_s(m_s) \propto m_s^\eta$  yields the CLF  $\propto L_s^{-1-0.9/\eta}$ . Therefore the above mass-luminosity relation implies the faint end slope of  $\sim -1.2$ . It is also found that even if we modify the value of  $\eta$  we cannot make the faint end slope shallower than  $-1$ . Hence to account for the observed trend we need extra mechanism. Following Cooray & Cen (2005), we introduce an efficient function to suppress the number of satellite galaxies in galactic halos:

$$f(m_s) = 0.5 \left[ 1 + \operatorname{erf}\left(\frac{\log m - \log m_c}{\sigma_m}\right) \right], \quad (12)$$

where  $\sigma_m = 1.5$  and the cutoff mass  $m_c$  depends on the host halo mass  $M$ :

$$m_c = 10^{11} h^{-1} M_\odot \exp\left[-\left(\frac{M}{5 \times 10^{13} h^{-1} M_\odot}\right)^2\right]. \quad (13)$$

For less massive ( $M \lesssim 10^{13} h^{-1} M_\odot$ ) halos, the efficiency function behaves as  $f(m_s) \rightarrow 0$  when  $m_s \ll 10^{11} h^{-1} M_\odot$  and  $f(m_s) \rightarrow 1$  when  $m_s \gg 10^{11} h^{-1} M_\odot$ . At cluster scales

$M \gtrsim 10^{14} h^{-1} M_\odot$  the efficiency function is almost always unity.

We neglect the redshift evolution of the relations presented in this section, since most lens galaxies are at  $z < 1$  where the evolution is expected to be mild.

#### 4 COMPUTING THE IMAGE SEPARATION DISTRIBUTION

To compute lensing cross sections, we have to convert galaxy luminosities to any quantities which characterize the mass distribution of galaxies. To do so, we use the scaling relations between the galaxy luminosity  $L$ , velocity dispersion  $\sigma$ , and effective radius  $R_0$ . Specifically, we adopt those derived from 9,000 early-type galaxies in the SDSS (Bernardi et al. 2003):

$$\frac{L}{10^{10.2} h_{70}^{-2} L_\odot} = \left(\frac{\sigma}{10^{2.197} \text{rms}^{-1}}\right)^{4.0}, \quad (14)$$

$$\frac{L}{10^{10.2} h_{70}^{-2} L_\odot} = \left(\frac{R_0}{10^{0.52} h_{70}^{-1} \text{kpc}}\right)^{1.5}, \quad (15)$$

where  $L$  is  $g$ -band galaxy luminosity and we defined  $h_{70} \equiv h/0.7$ . Note that the effective radius is related to the core radius of Hernquist profile (eq. [4]) by  $r_b = 0.551 R_0$ . For simplicity, we neglect tiny difference of  $b_J$ -band and  $g$ -band luminosities and regard  $L$  in the above equations as the same luminosities as those in §3. Although the fundamental plane can describe the correlation more tightly, we adopt these relations between two observables because they are much easier to handle. We also convert luminosities of galaxies to stellar masses assuming the universal stellar mass-to-light ratio of  $\Upsilon = 3.0 h_{70} M_\odot / L_\odot$ .

One of the most important ingredient in computing lensing probabilities is magnification bias which is determined by the source luminosity function. Below we assume a power-law  $\Phi(L) \propto L^{-\xi}$ , which makes the computation of magnification bias easier.

#### 4.1 Dark Halo Component

As discussed in §2.1, we use the improved adiabatic compression model of Gnedin et al. (2004) to compute the total mass distribution of a galaxy plus dark halo and hence to derive its lensing cross section. First, we derive the luminosity of a given halo with mass  $M$  using the mass-to-luminosity relation (9), and estimate the cooled baryon fraction  $f_b$  and the normalized core radius  $x_b$  from the stellar mass-to-light ratio  $\Upsilon$  and equation (15), respectively. From the mass distribution, we compute an image separation  $\theta$  and biased cross section  $\sigma_{\text{lens}}$ : We use approximations proposed by Oguri et al. (2002) to compute these quantities. Then the image separation distribution can be obtained by integrating the cross section:

$$\frac{dP_h}{d\theta} = \int dz_l (1+z_l)^3 \frac{cdt}{dz_l} \int dM \frac{dn}{dM} \sigma_{\text{lens}} \delta(\theta - \theta(M)). \quad (16)$$

The final probability distribution is obtained by averaging equation (16) over the probability distribution functions (PDFs) of the concentration parameter and the mass-to-luminosity relation.

#### 4.2 Subhalo Component

The projected mass distribution of a subhalo is approximated as the sum of an SIS and external convergence  $\kappa_{\text{ext}}$  originates from the mass associated with the host halo. We only consider the external convergence and neglect the effect of the external shear, since it has been shown that the external convergence is more effective to modify the image separation distribution (Oguri et al. 2005). From the velocity dispersion  $\sigma$ , the image separation  $\theta$  and the biased cross section  $\sigma_{\text{lens}}$  can be computed analytically (see Keeton & Zabludoff 2004, for the dependence on  $\kappa_{\text{ext}}$ ):

$$\theta = \frac{2\theta_E}{(1 - \kappa_{\text{ext}})} = \frac{8\pi (\sigma/c)^2 D_{\text{ls}}}{(1 - \kappa_{\text{ext}}) D_{\text{os}}}, \quad (17)$$

$$\sigma_{\text{lens}} = \pi (D_{\text{ol}}\theta_E)^2 \frac{2^\xi (1 - \kappa_{\text{ext}})^{-2(\xi-1)}}{3 - \xi}, \quad (18)$$

where  $D_{\text{os}}$  is the angular diameter distance from the observer to the source, etc. The external convergence is computed from the mass distribution of the host halo after baryon cooling (§2.1). Since the external convergence is written as a function of the projected radius  $R$ , the PDF of the external convergence becomes

$$p(\kappa_{\text{ext}}) d\kappa_{\text{ext}} = f_R(R) \frac{d\kappa_{\text{ext}}}{dR} dR, \quad (19)$$

where  $f_R(R)$  is the PDF of subhalos projected along line-of-sight, which we adopt the projected NFW profile with its concentration parameter given by equation (8):

$$f_R(R) dR = \frac{1}{h(c^*)} \int_{\phi_{\text{min}}}^{\pi/2} d\phi g \left( \frac{c^* R / r_{\text{vir}}}{\sin \phi} \right) \frac{c^*}{r_{\text{vir}}} dR, \quad (20)$$

$$\phi_{\text{min}} = \sin^{-1} \left( \frac{R}{r_{\text{vir}}} \right) \quad (21)$$

$$g(x) = \frac{x}{(1+x)^2}, \quad (22)$$

$$h(x) = \int_0^x dy g(y)$$

$$= \begin{cases} \frac{1}{1-x^2} \left[ -1 + \frac{2}{\sqrt{1-x^2}} \operatorname{arctanh} \sqrt{\frac{1-x}{1+x}} \right] & (x > 1) \\ \frac{1}{x^2-1} \left[ 1 - \frac{2}{\sqrt{x^2-1}} \operatorname{arctan} \sqrt{\frac{x-1}{x+1}} \right] & (x < 1). \end{cases} \quad (23)$$

From these, we compute the image separation distribution as

$$\frac{dP_s}{d\theta} = \int dz_l (1+z_l)^3 \frac{cdt}{dz_l} \int dM \frac{dn}{dM} \int dm_s f(m_s) \frac{dN}{dm_s} \times \int d\kappa_{\text{ext}} p(\kappa_{\text{ext}}) \sigma_{\text{lens}} \delta(\theta - \theta(\kappa_{\text{ext}})). \quad (24)$$

As in §4.1, the final probability distribution is obtained by averaging equation (24) over the PDFs of the concentration parameter of host halos (eq. [3]) and the mass-to-luminosity relation (eq. [11]). We set the upper limit of the integral over  $\kappa_{\text{ext}}$  to 0.9, because in the events beyond the limit ( $\kappa_{\text{ext}} \gtrsim 0.9$ ) subhalos should fall inside the critical radius of the host halo and therefore they should be included in lensing by dark halos computed in §4.1.

We note that the inclusion of the efficient function (eq. [12]) implies that a part of low-mass subhalos remains dark, i.e., does not harbor a galaxy. We neglect lensing by these dark subhalos because their contribution to total lensing probability distributions is rather small unless the inner profile of subhalos is very steep (Ma 2003; Li & Ostriker 2003).

The total image separation distribution is simply given by a sum of equations (16) and (24):

$$\frac{dP_t}{d\theta} = \frac{dP_h}{d\theta} + \frac{dP_s}{d\theta}. \quad (25)$$

## 5 THE IMAGE SEPARATION DISTRIBUTION

In this section, we compute image separation distributions for halos (central galaxies) and subhalos (satellite galaxies). In the specific examples below, we fix the source redshift to  $z_s = 2.0$  which is typical for lensed quasars. The magnification bias is computed assuming a power-law luminosity function with  $\xi = 2.1$  which is the luminosity function of the CLASS survey (Myers et al. 2003). First we will show the image separation distributions for dark halos and subhalos separately, and next we see the contribution of each component to the total distribution.

### 5.1 Dark Halo Component

Before going to the image separation distribution, we check the image separation as a function of halo masses to see the effect of baryon infall on lensing, which is shown in Figure 3. Two special cases are also shown for reference: One is neglecting baryon infall and leaving halos as NFW, and the other is adopting an SIS approximation with the velocity dispersion inferred from the luminosity of the central galaxy. It is found that the image separations agree well with those of SIS at low-mass ends, which is consistent with observations (e.g., Rusin et al. 2003; Rusin & Kochanek 2005). With increasing masses, image separations begin to deviate from SIS from  $\theta \sim 1''$  ( $M \sim 10^{12} h^{-1} M_\odot$ ). At  $\theta \gtrsim 10''$  ( $M \gtrsim 3 \times 10^{14} h^{-1} M_\odot$ ) image separations are quite similar to those of NFW. This figure justifies to some extent the two-population model in which SIS and NFW lenses are considered, but we note that at  $M \sim 10^{13} - 10^{14} h^{-1} M_\odot$

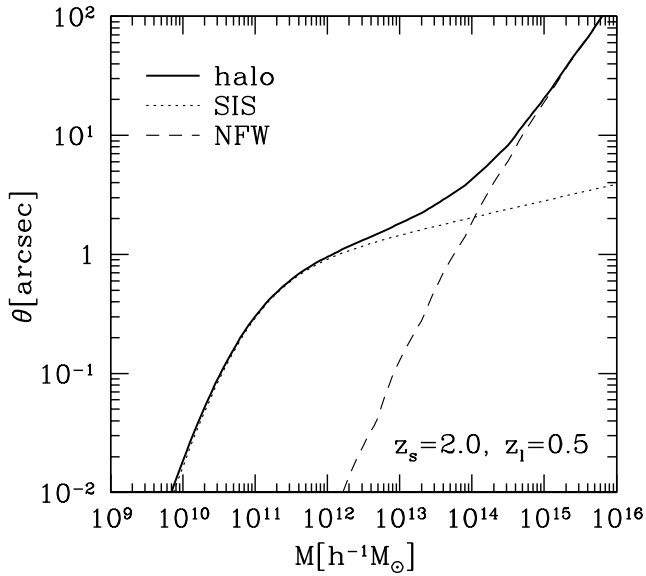


**Figure 3.** The image separations of lensing by dark halos after baryon cooling are plotted as a function of halo masses. In this plot, we do not take the PDFs of the mass-to-luminosity relation and concentration parameter into account. The lens redshift is fixed to  $z_l = 0.5$ . For comparison, we also show cases that we neglect baryon infall (NFW; *dashed line*) and we adopt an SIS approximation for the mass distribution of the halos after baryon infall (SIS; *dotted line*). Note that the velocity dispersion for SIS is derived from the scaling relation of equation (14).

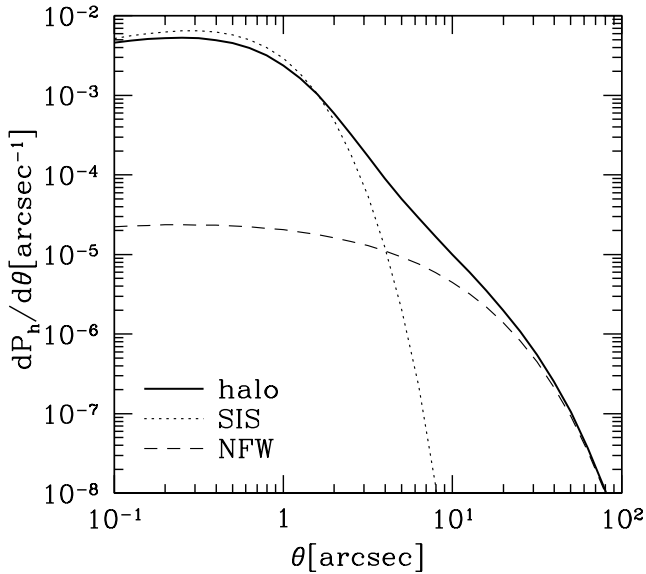


**Figure 4.** The image separation distribution from the dark halo component (eq. [16]). Lines are same as Figure 3.

things are too complicated to be described by such simple two-population model: Central galaxies are mainly responsible for lensing, but halo masses outside the lensing galaxies boost the image separation significantly, making the SIS approximation inaccurate.

We show the image separation distribution in Figure 4. As in Figure 3, at small- and large-separation regions the

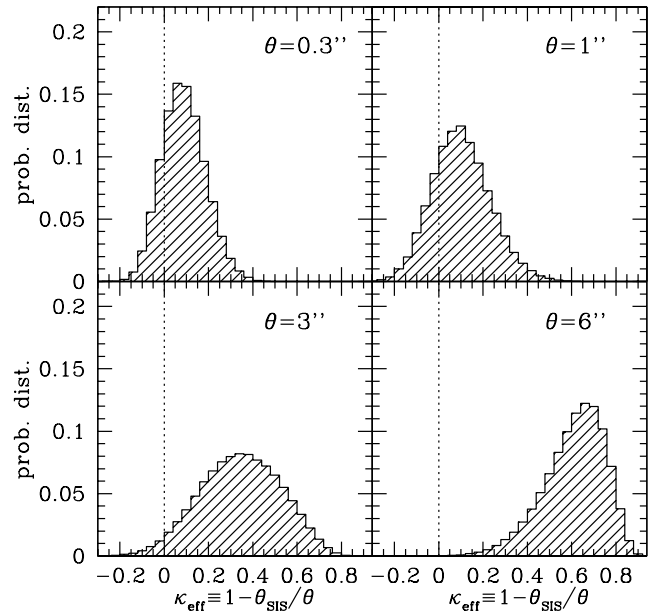


**Figure 5.** The probability distribution of “effective” external convergence  $\kappa_{\text{eff}}$  (eq. [26]) which is a measure of the deviation of the halo mass distribution from an SIS approximation of the corresponding central galaxy. We derive the distributions for several representative image separations:  $\theta = 0''.3$  (*upper left*),  $1''$  (*upper right*),  $3''$  (*lower left*), and  $6''$  (*lower right*).

probabilities are close to those of SIS and NFW, respectively, but at  $3'' \lesssim \theta \lesssim 10''$  it is difficult to describe lensing probabilities as either SIS or NFW alone. The lensing probabilities also differ from the sum of those of SIS and NFW. Therefore, we conclude that the image separation distribution cannot be described by a simple two-population model: We need to model the transition of halo mass distributions from SIS to NFW to predict correctly the distribution from small- to large-image separations.

We explore the transition from SIS to NFW more in terms of an “effective” external convergence defined by

$$\kappa_{\text{eff}} \equiv 1 - \frac{\theta_{\text{SIS}}}{\theta}, \quad (26)$$

where for each halo  $\theta_{\text{SIS}}$  is computed from the luminosity of the central galaxy via equation (14). The case  $\kappa_{\text{eff}} = 0$  means that the Einstein radius of the halo is exactly the same as that inferred from the luminosity of the central galaxy. The definition is motivated by the description of the image separation in the SIS plus external shear model (eq. [17]). We compute the PDFs of  $\kappa_{\text{eff}}$  for several representative image separations, which are shown in Figure 5. As expected, at  $\theta \lesssim 1''$  lens halos are on average close to an SIS, being consistent with observations (e.g., Rusin et al. 2003; Rusin & Kochanek 2005). However, at  $\theta \gtrsim 3''$  they clearly have larger image separations than those of corresponding SIS lenses. Therefore this Figure represents another case for the deviation from simple SIS lenses at that image separation region: At or beyond  $\theta \gtrsim 3''$  the image separations are enhanced significantly by surrounding dark halos.

We also point out that  $\kappa_{\text{ext}}$  has rather broad distributions even at small-separations  $\theta \lesssim 1''$ , which comes from the scatters of the concentration parameter (eq. [3])

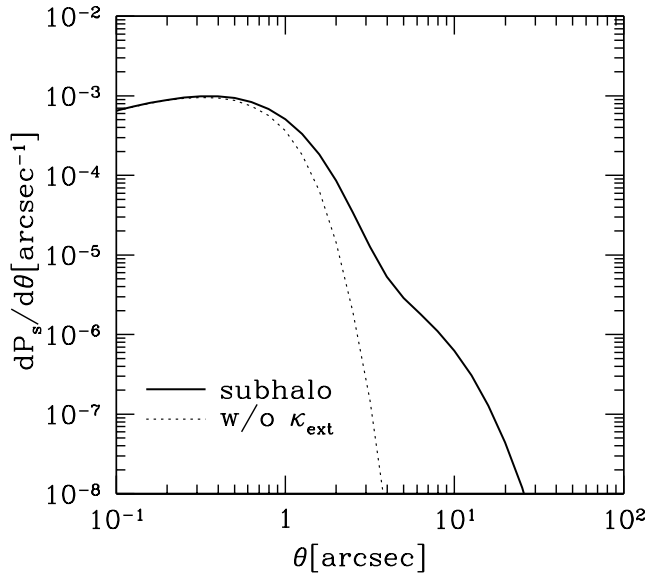


**Figure 6.** The image separation distribution from the subhalo component (eq. [24]) is plotted by a solid line. We also calculate the distribution without including  $\kappa_{\text{ext}}$ , which is shown by a dotted line.

and the mass-to-luminosity relation (eq. [11]) around their medians. This scatter around SIS approximations may be able to explain possible heterogeneous nature of lens galaxies inferred from the combination of gravitational lensing and stellar dynamics (Treu & Koopmans 2004) or time delay measurements between multiple images of lensed quasars (Kochanek et al. 2005).

## 5.2 Subhalo Component

We show the image separation distribution from the subhalo component in Figure 6. We find that the distribution has a peak at around  $\theta \sim 0.5''$ , and rapidly decreases with increasing  $\theta$ . It is also seen that the shape of the curve changes at around  $\theta \sim 5''$  over which the probability decreases less rapidly. We attribute this behavior to the contribution of very large external convergence ( $\kappa_{\text{ext}} \gtrsim 0.5$ ), because the probabilities are dominated by such extreme events (see below). This means that the result is somewhat sensitive to the upper limit of  $\kappa_{\text{ext}}$  which we set 0.9. However, as we will see in the next subsection, this does not cause any significant problems since at that image separation region the fraction of subhalo lensing in the total lensing probabilities are rather minor.

As shown in Oguri et al. (2005), the external convergence affects the image separation distribution significantly, particularly at the tail of the distribution  $\theta \gtrsim 3''$ . To show this explicitly, in Figure 6 we also plot the distribution without including  $\kappa_{\text{ext}}$ . It is found that the external convergence enhances the lensing probabilities at  $\theta \gtrsim 1''$  where the probabilities are decreasing function of  $\theta$ . This is consistent with the finding by Oguri et al. (2005). The enhancements are quite significant; factors of  $\sim 6$  at  $\theta = 2''$  and  $\sim 80$  at  $\theta = 3''$ . Note that these numbers are much larger than the results of Oguri et al. (2005), because here we concentrate on satellite galaxies that should have larger external conver-

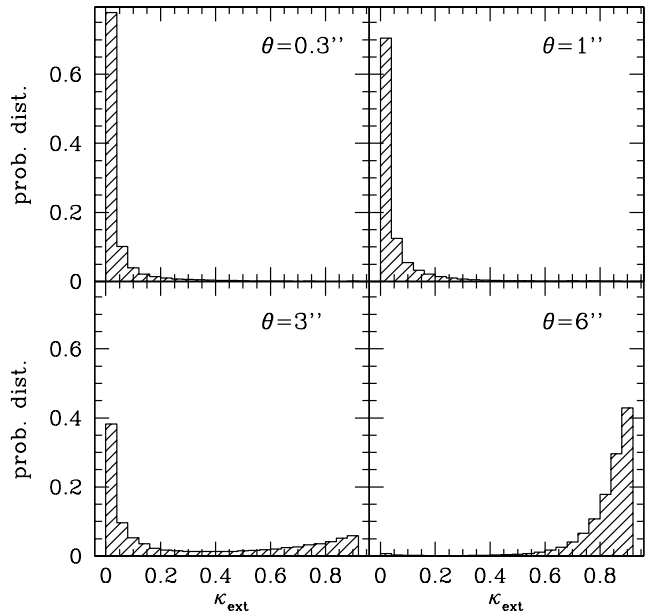


**Figure 7.** The distribution of external convergence  $\kappa_{\text{ext}}$  for the subhalo population. The PDFs for several different image separations are shown:  $\theta = 0.3''$  (upper left),  $1''$  (upper right),  $3''$  (lower left), and  $6''$  (lower right).

gence on average than central galaxies. Our result indicates that it is very important to include the external convergence of satellite galaxies, which originates from the host halo, to make reliable predictions of the image separation distribution for the subhalo component.

It is interesting to compute the posterior PDF of  $\kappa_{\text{ext}}$  to see expected environments of lensed satellite galaxies, as done by Oguri et al. (2005). In Figure 7, we show the PDFs for several different image separations. As expected, they are strong function of the image separation: Larger-separation lenses tend to lie in more dense environments. For instance, at  $\theta \lesssim 1''$  only  $\sim 10\%$  of lensing by satellite galaxies have large external convergence  $\kappa_{\text{ext}} > 0.1$ , while at  $\theta \sim 3''$  more than half of lenses are accompanied by such large external convergence. Lenses with  $\theta \sim 6''$  are dominated by those with very large  $\kappa_{\text{ext}}$ , which mean that lensing of such large image separations occurs only when satellite galaxies lie close to the center of their host halos on the projected two-dimensional lens plane.

## 5.3 Total Distributions

In this subsection, we put together the results in the previous subsections to derive the total image separation of strong lenses (eq. [25]).

Figure 8 plots the total image separation distribution as well as distributions for the halo and subhalo populations. We find that the halo population dominates the lensing probability at all image separations. However, the contribution of the subhalo population is also significant: The fraction takes the maximum value of  $\sim 0.2$  at around  $\theta = 1''$ , and decreases rapidly at  $\theta \gtrsim 3''$ . Therefore, we conclude that the subhalo population should not be ignored for the accurate prediction of the image separation distribution. Since

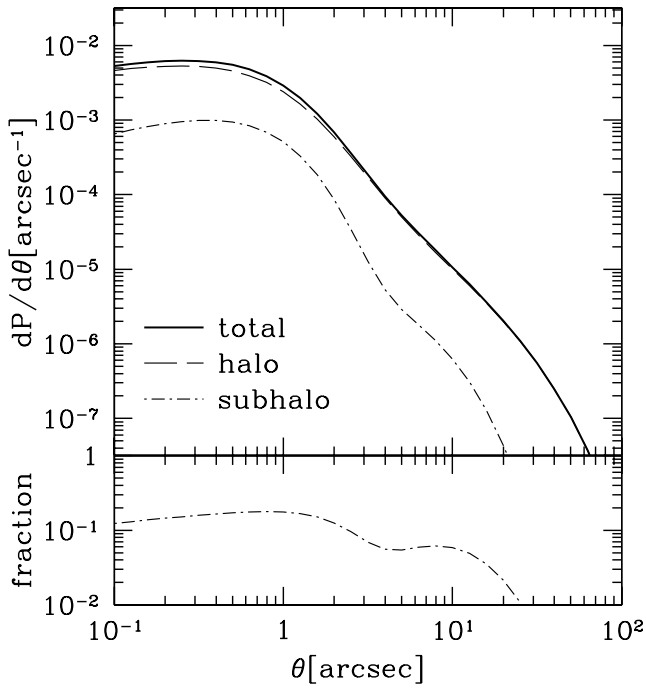


**Figure 8.** *Upper:* The total image separation distribution  $dP_t/d\theta$  (eq. [25]) is plotted by a solid line. The contributions of halo and subhalo components are also shown by dashed and dash-dotted lines, respectively. *Lower:* The ratio of the distribution for the subhalo population to the total distribution,  $(dP_s/d\theta)/(dP_t/d\theta)$ , is plotted as a function of the image separation.

most strong lenses have image separations of  $\sim 1'' - 2''$ , our model predicts that 10% – 20% of lenses are produced by satellite galaxies and 80% – 90% is caused by central galaxies.

An advantage of our halo approach is the ability to obtain further insight into the image separation distribution by computing the contribution of the image separation distribution from different mass intervals. For this purpose, we consider the following three types of halos, “galaxy” (defined by (host-)halos with masses of  $M < 10^{13} h^{-1} M_\odot$ ), “group” ( $10^{13} h^{-1} M_\odot < M < 10^{14} h^{-1} M_\odot$ ), and “cluster” ( $10^{14} h^{-1} M_\odot < M$ ), and explore the contribution of each type. We show the result in Figure 9. We find that the distributions of group and cluster have tails toward small-separations because of subhalo populations. Each type has quite similar distributions of the subhalo population, while those of the halo population are very different with each other. We also integrate the distributions over the image separation to estimate the fraction of each component to the total lensing probability, which is summarized in Table 1. Again, the fractions are very different for halo populations, but the differences are much smaller for subhalo populations. As a result, nearly half of lenses which lie in groups and clusters are caused by satellite galaxies (subhalos), in contrast with lenses in galactic halos which are dominated by the halo population. Finally, we compute fractions of lenses in lie in groups and clusters and find that they are  $\sim 14\%$  and  $\sim 4\%$ , respectively. These are roughly consistent with Keeton et al. (2000) who predicted that  $\sim 20\%$  and  $\sim 3\%$  of lenses lie in groups and clusters, respectively (a part of

**Table 1.** The fraction of lensing probabilities, integrated over the image separation. The entry “total” indicates a sum of lensing probabilities for halo and subhalo populations.

type ([ $h^{-1} M_\odot$ ])	galaxy ( $< 10^{13}$ )	group ( $10^{13} - 10^{14}$ )	cluster ( $> 10^{14}$ )
halo	0.74	0.08	0.02
subhalo	0.08	0.06	0.02
total	0.82	0.14	0.04

the differences may be ascribed to the different definitions of “group” and “cluster”).

How well does the total image separation distribution derived here account for observed image separation distributions? We compare our model prediction with the following two observed distributions:

- All 75 lensed quasars discovered to date. This sample includes both optical and radio lenses and are quite heterogeneous, but it has an advantage of the large number of lenses including several intermediate-separation lenses ( $3'' \lesssim \theta \lesssim 7''$ ) as well as one large-separation lens whose separation is  $\theta \sim 15''$ .
- 22 radio lenses discovered in the CLASS (Myers et al. 2003). Although this sample contains smaller number of lenses (and all lenses have  $\theta < 5''$ ), it is much more homogeneous and has well-defined selection functions. Although among the 22 lenses 13 were selected for a statistically well-defined subsample (Browne et al. 2003), we use all 22 lenses simply to increase statistics.

The results are shown in Figure 10. We find that our model explains both observed distributions reasonably well. An exception is that for all lenses the observed number of sub-arcsecond ( $\theta < 1''$ ) lenses appears to be smaller than expected. However, this is clearly due to a selection effect that sub-arcsecond lenses are difficult to find particularly in optical lens surveys. Indeed, for the CLASS lenses, which is a lens survey in a radio band, the discrepancy is less significant. Thus we conclude that our model well accounts for the observed image separation distributions.

It should be noted that the theoretical predictions is based on many assumptions. The most important ingredient of our model is the mass-to-luminosity relation defined in equations (9) and (10). To see how the result is dependent on the adopted relation, in Figure 11 we show the dependence of the total image separation distribution on the mass-to-luminosity relations. As seen in the Figure, the shape (rather than the overall normalization) of the image separation distribution is quite sensitive to the mass-to-luminosity relation. This indicates that precise measurements of the image separation distribution offer quite useful probe of the mass-to-luminosity relation.

## 6 SUMMARY AND DISCUSSIONS

In this paper, we have constructed a model of the image separation distribution. Our model is based on dark halos and subhalos which are linked to central and satellite galaxies respectively via simple mass-to-luminosity relation. For dark



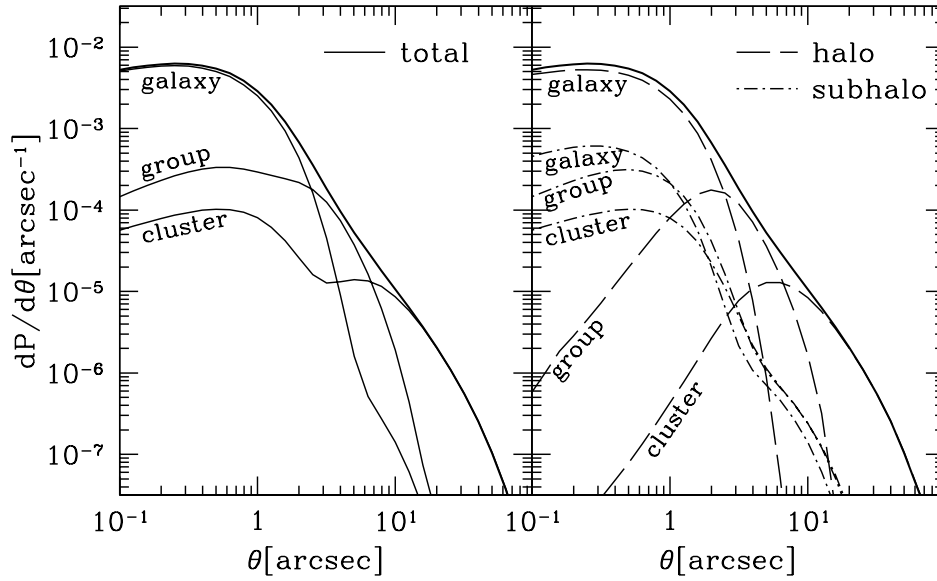


**Figure 9.** The contributions of different types of halos on the image separation distribution. We consider the following three types: “galaxy” which is defined by (host-)halos with masses of  $M < 10^{13} h^{-1} M_{\odot}$ , “group” by  $10^{13} h^{-1} M_{\odot} < M < 10^{14} h^{-1} M_{\odot}$ , and “cluster” by  $10^{14} h^{-1} M_{\odot} < M$ . *Left:* The total (halo plus subhalo populations) image separation for each type is plotted. The sum of distributions of three types is shown by thick solid line. *Right:* For each type, contributions of halo (*dashed*) and subhalo (*dash-dotted*) populations are shown separately.

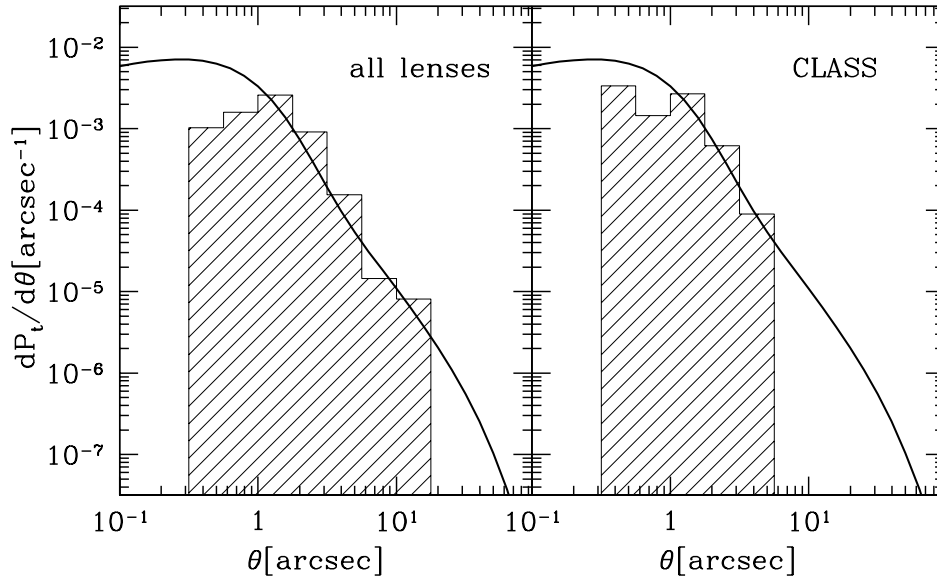


**Figure 10.** Observed image separation distributions (*histograms*) are compared with the theoretical prediction presented in Figure 8. We consider two observed distribution: (i) The distribution of all 75 lensed quasars discovered to date, and (ii) that of 22 lenses discovered in the CLASS (Myers et al. 2003). The observed distributions were shifted vertically to match their normalizations to the theoretical one.

halos and central galaxies, we have considered baryon cooling in a dark matter halo using an improved adiabatic contraction model of Gnedin et al. (2004). For satellite galaxies, we have considered the mass associate with their host halo. Our primary interest is to quantify the contribution of the subhalo population which has been ignored in all previous studies. Our results are summarized as follows:

- We predict that 80% – 90% of lenses should be caused by central galaxies (halos) and 10% – 20% of lenses should

be produced by satellite galaxies (subhalos). The fraction of the subhalo population takes the maximum at  $\theta \sim 1''$ , and becomes smaller with increasing image separations.

- The mass distributions of lensing halos at small ( $\theta \lesssim 3''$ ) and large ( $\theta \gtrsim 10''$ ) image separation regions are close to those of SIS and NFW, respectively. At  $3'' \lesssim \theta \lesssim 10''$  the mass distributions are complicated and cannot be described by either SIS or NFW.

- For both halo and subhalo populations, already at

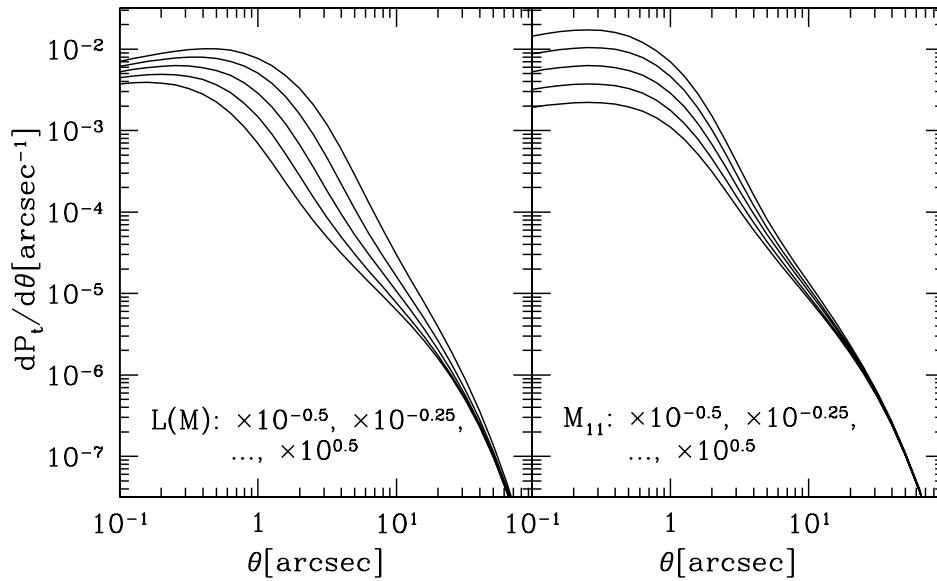


**Figure 11.** The dependence of the total image separation distribution on the mass-to-luminosity relations  $L(M)$  (eq. [9]) and  $L_s(M_s)$  (eq. [10]). *Left:* We change the overall normalizations of  $L(M)$  and  $L_s(M_s)$  by multiplying numerical factors to them. From upper to lower lines, we multiply  $10^{0.5}$ ,  $10^{-0.25}$ , 1,  $10^{-0.25}$ , and  $10^{-0.5}$ . *Right:* We shift the characteristic mass scale  $M_{11}$  and  $m_{11}$  in the mass-to-luminosity relations by multiplying the same factors to both  $M_{11}$  and  $m_{11}$  (upper lines correspond to the cases that smaller factors are multiplied).

$\theta \sim 3''$  the effect of dark halos becomes significant, making a simple SIS approximation worse. This means applying isothermal profiles to these lenses results in biased estimates of parameters such as velocity dispersions and the Hubble constant from time delays.

- Our model predicts that lensing halos of small separation lenses are heterogeneous: Halo-by-halo differences of the shape of rotation curves and the fraction of dark matter at image positions are large. This is a natural consequence of the scatters of the concentration parameter and the mass-to-luminosity relation around their medians.

- In computing the image separation distribution for the subhalo component, it is important to take account of the external mass which comes from their host halos. This also implies very strong dependence of environments of lensing satellite galaxies on image separation distributions.

- Halo and subhalo populations have quite different contributions of image separation distributions from different (host-)halo mass intervals. We predict that  $\sim 14\%$  of lenses lie in groups, and  $\sim 4\%$  in clusters. Almost half of lenses in groups and clusters are produced by satellite galaxies (sub-halos), rather than central galaxies (halos).

- We have compared our model predictions with observed image separation distributions and found that they are in reasonable agreements with each other. Since the shape of the image separation distribution is rather sensitive to the mass-to-luminosity relation, precise measurements of the image separation distribution in well-defined statistical lens samples offer powerful probe of the connection between dark halos and galaxies.

In summary, we have constructed a realistic model which predicts lensing probabilities from small to large image separations. The model is quite useful in understanding lens populations as a function of the image separation.

The fraction of lensing by the subhalo population, which has been derived for the first time in this paper, is important for not only an accurate prediction of the image separation distribution but also interpreting results of mass modeling of individual lens systems since central and satellite galaxies may show rather different lensing characteristics.

We note that there are several ways to improve our modeling. First, we have considered early-type galaxies only. Although this can be justified because most of lensing galaxies are early-type, the very existence of lensing by late-type galaxies indicates that the correct model needs to take both the two galaxy types into account. Since the lensing by spiral galaxies has quite small image separation  $\theta \lesssim 1''$  and also is inefficient (Keeton & Kochanek 1998), we expect that the inclusion of late-type galaxies decreases the number of sub-arcsecond lenses caused by central galaxies. In addition, we have neglected the scatters of the relations between galaxy luminosities, velocity dispersions, and effective radii. The scatters could affect the quantitative results, as the scatter in the mass-to-luminosity relation is important. The redshift evolutions of relations are also neglected. However, if we assume the evolution of early type galaxies at  $z \lesssim 1$  is purely passive, it implies that the mass distribution of lensing halos does not change across the redshift. Therefore we expect the effect of redshift evolution is rather small. More importantly, we have assumed simple spherical halos. In reality, dark halos are quite triaxial (Jing & Suto 2002) and the triaxiality enhances lensing probabilities by a few factors at large-separations (Oguri et al. 2003; Oguri & Keeton 2004; Hennawi et al. 2005a,b). On the other hand, small-separation lensing probabilities are hardly affected by the ellipticity of lens galaxies: Huterer et al. (2005) showed that the change is less than a few percents unless quasars are very bright. Large-

separation lensing probabilities are also sensitive to the inner slope of dark matter halos (e.g., Keeton & Madau 2001; Wyithe et al. 2001; Takahashi & Chiba 2001; Li & Ostriker 2002; Oguri 2002). We note, however, that the mass distribution after baryon cooling is rather insensitive to the inner slope of dark halos, thus the fraction of lensing by satellite galaxies does not depend on the inner slope very much. Refining our model by incorporating these is beyond the scope of this paper, but is of interest for future studies.

## ACKNOWLEDGMENTS

The author would like to thank C. Keeton, N. Dalal, J. Ostriker, J. Lee, and A. Vale for discussions. The author is supported by JSPS through JSPS Research Fellowship for Young Scientists.

## REFERENCES

- Bernardi M., et al., 2003, *AJ*, 125, 1849  
 Blumenthal G. R., Faber S. M., Flores R., Primack J. R., 1986, *ApJ*, 301, 27  
 Browne I. W. A., et al., 2003, *MNRAS*, 341, 13  
 Bullock J. S., Kolatt T. S., Sigad Y., Somerville R. S., Kravtsov A. V., Klypin A. A., Primack J. R., Dekel A., 2001, *MNRAS*, 321, 559  
 Chen D.-M., 2004, *A&A*, 418, 387  
 Chen D.-M., 2005, *ApJ*, 629, 23  
 Cooray A., Milosavljević M., 2005, *ApJ*, 627, L89  
 Cooray A., Cen R., 2005, *ApJ*, 633, L69  
 De Lucia G., Kauffmann G., Springel V., White S. D. M., Lanzoni B., Stoehr F., Tormen G., Yoshida N., 2004, *MNRAS*, 348, 333  
 Gao L., White S. D. M., Jenkins A., Stoehr F., Springel V., 2004, *MNRAS*, 355, 819  
 Gnedin O. Y., Kravtsov A. V., Klypin A. A., Nagai D., 2004, *ApJ*, 616, 16  
 Hennawi J. F., Dalal N., Bode P., Ostriker J. P., 2005a, *ApJ*, submitted (astro-ph/0506171)  
 Hennawi J. F., Dalal N., Bode P., 2005b, *ApJ*, submitted (astro-ph/0506175)  
 Hernquist L., 1990, *ApJ*, 356, 359  
 Huterer, D., Ma, C.-P., 2004, *ApJ*, 600, L7  
 Huterer, D., Keeton, C. R., & Ma, C.-P. 2005, *ApJ*, 624, 34  
 Inada N., et al., 2003, *Nature*, 426, 810  
 Jing Y. P., Suto, Y., 2002, *ApJ*, 574, 538  
 Keeton C. R., 2001, *ApJ*, 561, 46  
 Keeton C. R., Christlein D., Zabludoff A. I., 2000, *ApJ*, 545, 129  
 Keeton, C. R., & Kochanek, C. S. 1998, *ApJ*, 495, 157  
 Keeton C. R., Madau P. 2001, *ApJ*, 549, L25  
 Keeton C. R., Zabludoff A. I., 2004, *ApJ*, 612, 660  
 Kochanek C. S., White M., 2001, *ApJ*, 559, 531  
 Kochanek C. S., Morgan N. D., Falco E. E., McLeod B. A., Winn J. N., Dembicky J., Ketzeback B., 2005, *ApJ*, submitted (astro-ph/0508070)  
 Kuhlen M., Keeton C. R., Madau P., 2004, *ApJ*, 601, 104  
 Li L.-X., Ostriker J. P., 2002, *ApJ*, 566, 652  
 Li L.-X., Ostriker J. P., 2003, *ApJ*, 595, 603  
 Ma, C.-P., 2003, *ApJ*, 584, L1  
 Myers S. T., et al., 2003, *MNRAS*, 341, 1  
 Narayan R., White S. D. M., 1988, *MNRAS*, 231, 97P  
 Navarro J. F., Frenk C. S., White S. D. M., 1997, *ApJ*, 490, 493  
 Oguri M., 2002, *ApJ*, 580, 2  
 Oguri M., et al., 2004, *ApJ*, 605, 78  
 Oguri M., Keeton C. R., 2004, *ApJ*, 610, 663  
 Oguri M., Keeton C. R., Dalal N., 2005, *MNRAS*, 364, 1451  
 Oguri M., Lee J., 2004, *MNRAS*, 355, 120  
 Oguri M., Lee J., Suto Y., 2003, *ApJ*, 599, 7  
 Oguri M., Taruya A., Suto Y., Turner E. L., 2002, *ApJ*, 568, 488  
 Porciani C., Madau P., 2000, *ApJ*, 532, 679  
 Press W. H., Schechter P., 1974, *ApJ*, 187, 425  
 Reed D., Gardner J., Quinn T., Stadel J., Fardal M., Lake G., Governato F., 2003, *MNRAS*, 346, 565  
 Rusin D., Kochanek C. S., Keeton C. R., 2003, *ApJ*, 595, 29  
 Rusin D., Kochanek C. S., 2005, *ApJ*, 623, 666  
 Sarbu N., Rusin D., Ma C.-P., 2001, *ApJ*, 561, L147  
 Sheth R. K., et al., 2003, *ApJ*, 594, 225  
 Sheth R. K., Tormen G., 1999, *MNRAS*, 308, 119  
 Takahashi R., Chiba T., 2001, *ApJ*, 563, 489  
 Treu T., Koopmans L. V. E., 2004, *ApJ*, 611, 739  
 Turner E. L., Ostriker J. P., Gott J. R., 1984, *ApJ*, 284, 1  
 Vale A., Ostriker J. P., 2004, *MNRAS*, 353, 189  
 van den Bosch F. C., Yang X., Mo H. J., Norberg P., 2005, *MNRAS*, 356, 1233  
 Walsh D., Carswell R. F., Weymann R. J. 1979, *Nature*, 279, 381  
 Wyithe J. S. B., Turner E. L., Spergel D. N., 2001, *ApJ*, 555, 504  
 Yang X., Mo H. J., van den Bosch F. C., 2003, *MNRAS*, 339, 1057  
 Zhang T.-J., 2004, *ApJ*, 602, L5  
 Zhang T.-J., Yang Z.-L., He X.-T., 2005, *MPLA*, 20, 851